Journal of Contaminant Hydrology 265 (2024) 104391

Contents lists available at ScienceDirect

Journal of Contaminant Hydrology

journal homepage: www.elsevier.com/locate/jconhyd

# Contaminant mobilization from the vadose zone to groundwater during experimental river flooding events

Rakiba Sultana [a,*], Raymond H. Johnson [b], Aaron D. Tigar [b], Timothy J. Wahl [c], Cullen E. Meurer [a], Kendyl N. Hoss [a], Shangping Xu [a], Charles J. Paradis [a]

[a] Department of Geosciences, University of Wisconsin-Milwaukee, 3209 N. Maryland Ave, Milwaukee, WI 53211, United States
[b] RSI EnTech, LLC, Contractor to the U.S. Department of Energy Office of Legacy Management, 2597 Legacy Way, Grand Junction, CO 81503, United States
[c] School of Freshwater Sciences, University of Wisconsin-Milwaukee, 600 E Greenfield Ave, Milwaukee, WI 53204, United States

ARTICLE INFO

*Keywords:*
Groundwater contamination
In-situ tracer experiment
Contaminant-rich pore water
Evaporite salts
Breakthrough curves

ABSTRACT

Natural river flooding events can mobilize contaminants from the vadose zone and lead to increased concentrations in groundwater. Characterizing the mass and transport mechanisms of contaminants released from the vadose zone to groundwater during these recharge events is particularly challenging. Therefore, conducting highly-controlled in-situ experiments that simulate natural flooding events can help increase the knowledge of where contaminants can be stored and how they can move between hydrological compartments. This study specifically targets uranium pollution, which is accompanied by high sulfate levels in the vadose zone and groundwater. Two novel experimental river flooding events were conducted that utilized added non-reactive halides (bromide and iodide) and 2,6-difluorobenzoate tracers. In both experiments, about 8 $m^3$ of traced water from a nearby contaminant-poor river was flooded in a 3-m diameter basin and infiltrated through the vadose zone and into a contaminant-rich unconfined aquifer for an average of 10 days. The aquifer contained 13 temporary wells that were monitored for solute concentration for up to 40 days. The groundwater analysis was conducted for changes in contaminant mass using the Theissen polygon method and for transport mechanisms using temporal moments. The results indicated an increase in uranium (21 and 24%), and sulfate (24 and 25%) contaminant mass transport to groundwater from the vadose zone during both experiments. These findings confirmed that the vadose zone can store and release substantial amounts of contaminants to groundwater during flooding events. Additionally, contaminants were detected earlier than the added tracers, along with higher concentrations. These results suggested that contaminant-rich pore water in the vadose zone was transported ahead of the traced flood waters and into groundwater. During the first flooding event, elevated concentrations of contaminants were sustained, and that chloride behaved similarly. The findings implied that contaminant- and chloride-rich evaporites in the vadose zone were dissolved during the first flooding event. For the second flooding event, the data suggested that the contaminant-rich evaporites continued to dissolve whereas chloride-rich evaporites were previously flushed. Overall, these findings indicated that contaminant-rich pore water and evaporites in the vadose zone can play a significant role in contaminant transport during flooding events.

## 1. Introduction

Flooding is a dynamic event with rapidly changing flows, chemical compositions, and sediment loads (Simpson et al., 2013). An extreme flooding event can result in a significant mobilization and redistribution of contaminants, leading to both socio-economic and environmental damage (Crawford et al., 2022; Ponting et al., 2021). When a soil floods, the mobility of contaminants can either increase or decrease based on soil mineralogy and texture, the properties that change spatially (Ponting et al., 2021). This phenomenon is particularly critical because when mobilized downward, contaminants can potentially persist for long time periods within the subsurface and become a continuing source of contamination to groundwater (Truex et al., 2009). As such, water quality is dependent on the interplay between river-groundwater-vadose zone system (Yabusaki et al., 2017).

The subsurface hydrogeological layers - the saturated zone

* Corresponding author.
*E-mail address:* sultana.rakiba151@gmail.com (R. Sultana).

https://doi.org/10.1016/j.jconhyd.2024.104391
Received 19 April 2024; Received in revised form 8 June 2024; Accepted 22 June 2024
Available online 24 June 2024

(groundwater occurrence), unsaturated zone, and capillary fringe (Freeze and Cherry, 1979), play crucial roles in controlling water movement and quality in the river-groundwater-vadose zone system (Yabusaki et al., 2017). The saturated zone lies below the water table and comprises soil pores filled with water under positive pressure head. The capillary fringe, situated above the water table contains soil pores filled with water but has pressure heads less than atmospheric. The unsaturated zone is above the capillary fringe, with soil pores that are not fully saturated and have negative pressure heads. Grouped together, in this study, the capillary fringe and unsaturated zone are referred to as the vadose zone that occurs above the water table and is under negative pressure head. The water table, defined as the surface where the fluid pressure is exactly atmospheric, separates the vadose zone from the saturated zone, where groundwater occurs. Understanding the dynamics between these layers is essential to identifying contaminant storage in the subsurface and comprehending the factors responsible for subsequent contaminant release during flooding events.

To understand the factors contributing to contaminant transport from the vadose zone to groundwater during a flooding event, continuous real-time physio-chemical data from the floodplain is required (Barber et al., 2017). Due to the unpredictability in the frequency and magnitude of occurrence of a flooding event, there is usually an absence of the baseline and continuous physio-chemical data during the event (Ponting et al., 2021). Occasionally, baseline data from pre- and post-natural events are established (U.S. Department of Energy, 2019) but it is usually difficult to use these data to assess the processes of events and their potential impacts (Ponting et al., 2021). Many of the findings on contaminant mobility during flooding events, therefore, are based on direct collection of time-series groundwater samples under normal flow and during inundations (Barber et al., 2017; U.S. Department of Energy, 2019; Yang et al., 2023). While these data can provide real-time physio-chemical data during a flooding event, controlled experiments can provide more robust understanding of the underlying processes of contaminant transport during the events by reducing uncertainties in evaluation of the recharge processes (Ofer Dahan et al., 2007; Ponting et al., 2021).

Some of the controlled experiments that are available on mobility of contaminants on floodplain soils are based on generating artificial flooding environments in the laboratory (Frohne et al., 2011; Izquierdo et al., 2017; Weber et al., 2009). Laboratory column experiment has also been performed to analyze solute migration through the vadose zone and groundwater during flash floods (Amiaz et al., 2011). Although the laboratory-based studies can provide insights into the processes occurring during the course of the flooding events, these findings are difficult to extrapolate to field-scale interpretations (Hooda, 2010). In contrast, on-site experiments on the effect of flooding events on contaminant mobility in floodplain soils can better provide results on effects of flooding events on groundwater (Ponting et al., 2021). There are few studies that conducted field scale infiltration experiments to evaluate dynamics of flood water percolation and groundwater recharge via variation in the vadose zone water content profile (Benito et al., 2010; Dahan et al., 2008; Ofer Dahan et al., 2007). The dynamics of percolating flood water flow and subsequent contaminant transport through the vadose zone was first studied by multi-tracer field infiltration experiment in an alluvium underlying a stream channel (Dahan et al., 2009). These studies based on field infiltration experiments provided transient data on water percolation and contaminant migration during flooding events. However, river water was not utilized as the infiltration source in these field experiments, and the analysis did not specifically focus on reactive solute transport when examining contaminant transport during flooding events.

Contaminants such as uranium and sulfate, are highly reactive and are more mobile during oxic conditions such as a flooding event, than reducing conditions (Langmuir, 1977). Sulfate is also very soluble in groundwater and can travel a long distance in subsurface environments (Miao et al., 2012). Moreover, sulfate is a common anion in soluble-prone evaporite minerals and can potentially entrap uranium in dry conditions and subsequently release during groundwater recharge (Apaydın and Aktaş, 2012; Carlisle et al., 1978). In addition, uranium is considered a primary contaminant in groundwater; primary contaminants pose significant health risks, for which the United States Environmental Protection Agency (EPA) sets enforceable Maximum Contaminant Levels (MCLs) under the Safe Drinking Water Act (National Primary Drinking Water Regulations, 2024). On the other hand, sulfate is considered a secondary contaminant in groundwater; secondary contaminants are not directly harmful to human health but can affect the aesthetic qualities of water, such as taste, odor, colour, and staining, with the EPA setting non-enforceable guidelines called Secondary Maximum Contaminant Levels (SMCLs) (Drinking Water Regulations and Contaminants, 2024). Given the complex geochemistry of contaminants like uranium and sulfate, especially their sensitivity to redox conditions and pH, it is crucial to understand their behavior during floods (Langmuir, 1977). To our knowledge, controlled in-situ flooding experiments have not been conducted to describe reactive contaminant transport behavior during the course of a flooding event.

In the present work, two in-situ experiments, the first of their kind, were performed to simulate flooding events at a contaminated field site to study contaminant behavior across hydrogeological compartments during the events. In the first flooding experiment non-reactive tracers (halides and fluorobenzoates) were utilized to contrast contaminant behavior with non-reactive tracers during floods. In the second flooding experiment, alkalinity was added along with a non-reactive tracer (halide) to suggest possible remediation of the contaminated site. The specific objectives of our study were to (1) identify the hydrogeological compartment(s) responsible for the contaminant transport, and (2) elucidate the dominant mobilization mechanisms of contaminants during floods. Significant past research (Johnson et al., 2016; Paradis et al., 2022a; U.S. Department of Energy, L.M, 2014) allowed us to hypothesize that contaminants mobilize from the vadose zone due to contaminant-rich evaporite dissolution during a flooding event. Overall, our study presents new results from the experimentally simulated floods at a field scale and can inform the development of predictive models for groundwater management.

## 2. Materials and methods

### 2.1. Study site

The study site is in central Wyoming (WY), 2 miles southwest of Riverton and on river alluvium between the Wind River and Little Wind River (Fig. S1). There are three aquifers at the site which are: (1) an unconfined aquifer, (2) a semiconfined aquifer, and (3) a confined aquifer (Fig. 1a). The unsaturated zone is composed of approximately 1.2–1.5 meters (m) of silt and clay. The shallow aquifer consists of approximately 4.5–6 m of sand and gravel, and the semiconfined and confined aquifers comprise the upper units of the Early Eocene Wind River Formation, which is over 150 m thick in the vicinity of the site (Dam et al., 2015). The predominant stratigraphic unit of Early Eocene Wind River Formation is composed of sandstone, conglomerate, siltstone, and claystone (Keefer, 1970). The Wind River Formation was accumulated through the action of fluvial systems that transported debris to the Wind River Basin located to the north. Regionally, the deposition of the formation occurred on an erosional surface sloping towards the north, situated between the Granite Mountains to the south and the depression of the Wind River Basin to the north (Robert W. Gregory, 2019).

The Riverton Processing site, formerly a uranium mill tailings facility operating from 1958 to 1963 (U.S. Department of Energy, 2016) is currently among 107 sites managed by the United States (U.S.) Department of Energy across the U.S., aimed at restoring sites contaminated due to nuclear production activities (Dwivedi et al., 2022). The primary source of contamination to the surface and shallow

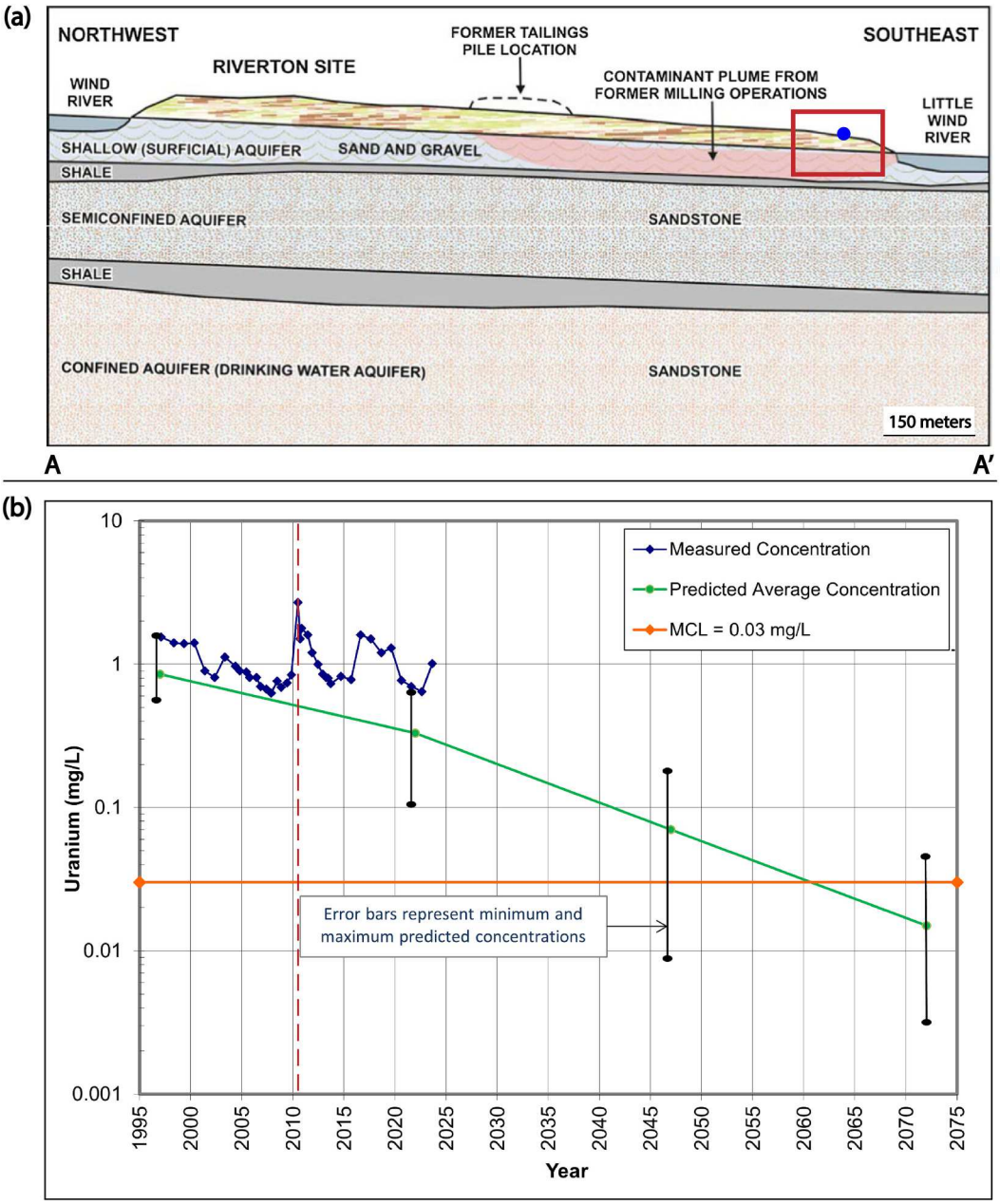


**Fig. 1.** (a) Cross-sectional area, AA' of the study area (Fig. S1) (Dam et al., 2015). The red rectangle shows the downgradient location where the two field experiments were performed. The blue dot shows the approximate location of the flood basin (Fig. 2). (b) Comparisons between the GANDT model predictions and actual groundwater concentrations at Riverton, WY, in 1998. Uranium concentration spike in groundwater during flooding in 2010 is indicated by red dotted line. (For interpretation of the references to colour in this figure legend, the reader is referred to the web version of this article.)

groundwater beneath and downgradient of the site was the tailings slurry from the former mill (Fig. 1a). Surface remediation was completed in 1989 by removing the tailings to radioactivity standards for radium (Narasimhan et al., 1986; White et al., 1984). Despite these measures, substantial concentrations of solid-phase contaminants are present in both the vadose zone and aquifer sediments at our study area (Paradis et al., 2022a; U.S. Department of Energy, 2016). Due to the presence of shale layers (Fig. 1a), confined aquifer remains uncontaminated and mill-related contaminants are not detected in the semiconfined aquifer. However, the surficial unconfined aquifer is contaminated with uranium (~1.7 milligrams/liters [mg/L]), and sulfate (~6300 mg/L) concentrations (U.S. Department of Energy, 2016) exceeding regulatory limits. Uranium has a maximum concentration limit (MCL) of 0.03 mg/L (National Primary Drinking Water Regulations, 2024) and sulfate has a secondary MCL of 250 mg/L (Drinking Water Regulations and Contaminants, 2024) in groundwater. The major dissolved uranium species, as determined using the PHREEQC 3.7.3 with the LLNL database (Input file. S1), in the groundwater of the site are $UO_2SO_4$, $UO_2(SO_4)_2^{2-}$, $UO_2(CO_3)_3^{4-}$, $UO_2(CO_3)_2^{2-}$, $UO_2CO_3$ and $UO_2(OH)_2$. For sulfur, the main dissolved species is $SO_4^{2-}$, with no significant precipitation of sulfate-bearing minerals, as indicated by the saturation indices (SI) of anhydrite (−0.41), gypsum (−0.15), bloedite (−6.32), and epsomite (−2.56) in the aquifer sediments. The groundwater plume was estimated to be attenuated below MCLs through natural flushing within the past 100 years from 1997, according to the Riverton Groundwater Analysis and Network Design Tool (GANDT) model simulated by Sandia National Laboratories (Knowlton Jr et al., 1997; U.S. Department of Energy, 1998). The GANDT code incorporated groundwater flow and transport

uncertainty through Monte Carlo simulations, accounting for concentration data and spatial variability using geostatistical methods while employing a single sorption partitioning coefficient (Kd) approach. However, the annual monitoring indicated persistence of the plume, including an increase in uranium concentration following a flooding event in 2010 (Fig. 1b). The discrepancy between the model predictions and observational data caused concern for the longevity of the contaminant plume and exhibited lapses in the knowledge of the processes governing contaminant storage and release (Dam et al., 2015).

Given the arid climate and dry summer in Riverton, evaporite deposits are prevalent especially in the upper vadose zone due to high evapotranspiration, particularly along south-facing riverbanks on the north side of the Little Wind River (Looney et al., 2014; U.S. Department of Energy, L.M, 2014). These deposits, primarily consisting of halite (NaCl), blödite ($Na_2Mg(SO_4)_2{\cdot}4(H_2O)$), and thenardite ($Na_2SO_4$) are widespread in the vadose zone (Management, 2016). The sulfate-bearing evaporites collected along the river in 2014 (Fig. S2) indicated uranium (0.0014 to 0.066 g/kg), and sulfate (5.4 to 2200 g/kg) from following strong acid digestion of the evaporite samples (Management, 2016; U.S. Department of Energy, L.M, 2014). Based on the data, previous researchers suggested that these evaporite minerals present in the vadose zone could serve as a secondary source of persistent contaminant plumes (Dam et al., 2015; Johnson et al., 2016).

Prior to conducting our flooding experiments in 2020 (August 3–October 4) and 2021 (August 1–September 10), an in-situ tracer injection experiment directly to the aquifer was performed in 2020 (July 17–July 31) within the same area of interest as our study (Fig. 2). The goal of the injection experiment was to investigate contaminant (uranium) behavior solely in the aquifer during a flood (Paradis et al., 2022a). The injection experiment was initiated by directly injecting traced river water into the groundwater through well 1001 (Fig. 2b). The injection phase was followed by sampling and analysis of the tracers in the 13 monitoring wells (Fig. 2b) under natural-gradient conditions for 18 days.

In the present study, contaminant mobility is investigated through two tracer flooding experiments with river water (flood water) percolating through the vadose zone and downward into the groundwater.

### 2.2. Experimental flooding events

Two tracer field experiments (Table 1), each simulating a flooding event, were conducted near the banks of Little Wind River, Riverton, WY (Fig. 1). A series of 13 temporary monitoring wells (Fig. 2) were installed by direct push and screened across the water Table A 3 m (m) diameter basin was placed upgradient of the wells. About 8 $m^3$ of river water (flood water) was filled in an infiltration tank (Fig. 1). Specific field and laboratory measurements with corresponding instruments and the relevant information of added tracers and alkalinity are listed in Table S1 and Table S2. The hydrochemistry of the river water (flood water) was different in composition than that of groundwater (Table S3). The typical depth of the water table was between 2 and 2.5 m below ground surface (bgs) during the experiments. The wells were installed as three transects oriented perpendicular to groundwater flow, i.e., southwest to northeast. The target screen interval for the temporary gallery wells was between 2 and 3.5 m bgs. The total distance between the first and last transects was 3 m with uniform spacing in between wells to allow for the transport of the tracer to be completed within a reasonable timeframe. Borehole dilution, slug testing, and groundwater pumping tests were completed before any tracer testing to get groundwater hydraulic conductivity estimates (U.S. Department of Energy, 2023). The average linear groundwater velocity was estimated at 0.2 to 0.3 m/day from a field tracer test performed prior to the injection experiment and our flooding experiments to investigate physical properties (groundwater velocity and matrix diffusion) of the uranium-contaminated aquifer (Paradis et al., 2022b). Matrix diffusion affects the migration of contaminants from the mobile zone to adjacent immobile zones of the porous matrix and vice versa, thereby impacting contaminant travel times by spreading contaminants over a larger volume of the subsurface (Paradis et al., 2020).

In Flood-1, two non-reactive solute tracers, lithium bromide (LiBr) and sodium 2,6-difluorobenzoate (NaDFB), each with different aqueous diffusion coefficients, were introduced into the flood water in the infiltration tank (Fig. 2a). The water from the tank was then pumped into the flood basin (Fig. 2a) using a peristaltic pump over a period of approximately 8 days. This process allowed the tracers to travel through the vadose zone and into the contaminant-rich unconfined aquifer. Difluorobenzoate has a much lower aqueous diffusion coefficient ($7.2 \times 10^{-10}$ $m^2/s$) (Bowman and Gibbens, 1992) than bromide ($21 \times 10^{-10}$ $m^2/s$) (Callahan et al., 2000). The presence of matrix diffusion would result in a relatively lower peak concentration and longer mean arrival time of bromide than difluorobenzoate. Thus, the difference between the diffusion coefficient was used to characterize any mass transport of solutes from mobile to immobile zones due to molecular diffusion, i.e., matrix diffusion, in the groundwater (Paradis et al., 2020). However, the non-reactive tracers, bromide, and difluorobenzoate, employed in Flood-1 demonstrated similar behavior (Fig. S3), suggesting negligible

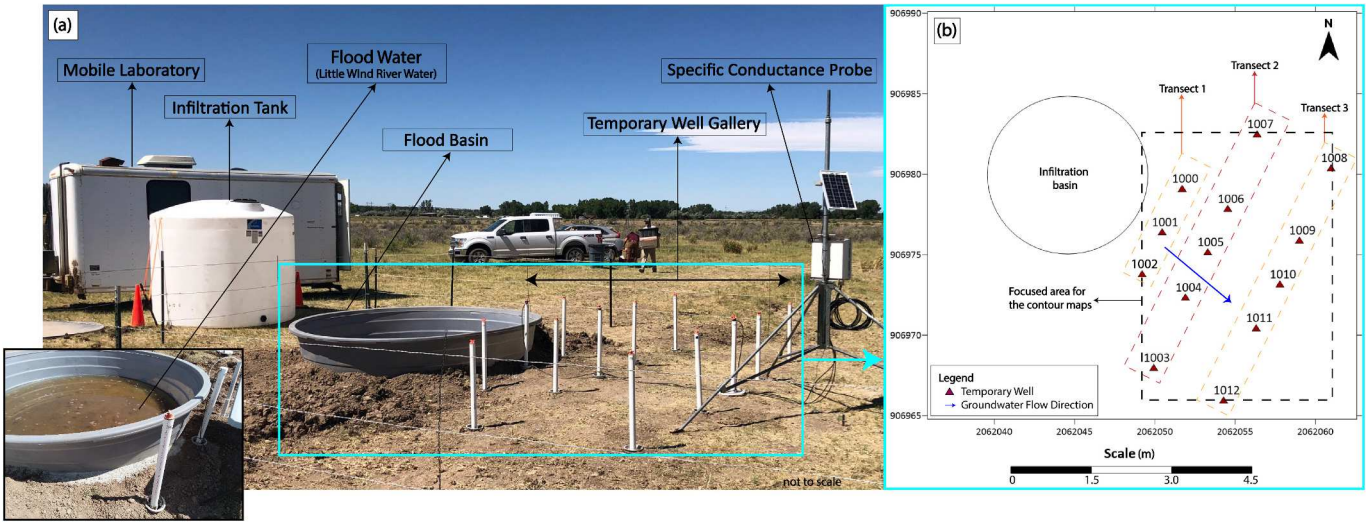


**Fig. 2.** (a) 13 monitoring wells and a flood basin at the experimental location and, (b) experimental set-up for two consecutive floodings at the site. The inset at the left bottom corner shows the flood basin with traced river water after initiating the experiment.

**Table 1**
Summary of two tracer field experiments conducted in 2020 (Flood-1) and 2021 (Flood-2).

| Experiment | Water | Rate | Flooded | Tracers | Alkalinity | Sampled |
|---|---|---|---|---|---|---|
| (#) | Source ($m^3$) | ($m^3$/h) | (days) | Type (g) | Type (g) | (months) |
| Flood-1 | Little Wind River (~8 $m^3$) | 0.041 | ~8 | Bromide (948) DFB (979) | None Added | ≈2 |
| Flood-2 | | 0.027 | ~12 | Iodide (2117) | $NaHCO_3$ (20,000) | ≈1 |

matrix diffusion in our study. Since there was no discernible difference between the transport behavior of two tracers, bromide was selected for discussions pertaining to Flood-1. Following the completion of Flood-1 in summer 2020, Flood-2 was performed in summer 2021 at the same location. Flood-2 was done with added alkalinity, sodium bicarbonate ($NaHCO_3$), to investigate its influence on uranium mobility. A different artificial non-reactive solute tracer, sodium iodide (NaI) was used in Flood-2 to differentiate between Flood-1 and Flood-2 when analyzing the traced groundwater. NaI and $NaHCO_3$ were added to flood water similarly as Flood-1 and flooded into the basin for about 12 days. Notably, before both flooding experiments, an injection experiment was performed directly into the same aquifer as this study (Paradis et al., 2022a; U.S. Department of Energy, 2023). This injection experiment applied NaI and potassium pentafluorobenzoate (KPFB) to study contaminant release solely from the aquifer. The experiment did not observe any difference in the behavior of iodide and pentafluorobenzoate (Fig. S4), suggesting that iodide behaved conservatively during the injection experiment. Daily static water levels were measured, and samples were collected via peristaltic pumps under low-volume and low-flow conditions at 100 mL/min. Samples were measured immediately for temperature, specific conductance, pH, dissolved oxygen (DO), ferrous iron, alkalinity, and oxidation-reduction potential. Laboratory analyses for uranium and other metals was completed at the U.S. Department of Energy Office of Legacy Management Environmental Sciences Laboratory, Los Alamos National Laboratory and University of Wisconsin-Milwaukee. More detailed information on the field methods is available in the relevant documentation for the study (U.S. Department of Energy, 2023).

### 2.3. Data analyses

#### 2.3.1. Temporal analyses

Breakthrough curves of potentially reactive solutes, chloride (Cl), uranium (U), sulfate ($SO_4$), sodium (Na), magnesium (Mg), potassium (K), calcium (Ca), manganese (Mn), and molybdenum (Mo), were constructed and plotted for concentrations in groundwater (pre flooding), observed (during and post flooding), expected, and flood water (infiltrated river water). Breakthrough curves for $Fe^{2+}$ were not considered due to being below the detection limit (0.03 mg/L). Similarly, the total Fe ($Fe^{2+}$+$Fe^{3+}$) data was disregarded due to its noisy signals. The breakthrough curves of non-reactive added tracers, bromide (Br) in Flood-1 and iodide (I) in Flood-2 were not constructed explicitly since their concentrations were used to calculate the expected concentrations of the reactive solutes (Paradis et al., 2019). Moreover, in Flood-1, bromide and difluorobenzoate behaved similarly so only bromide concentrations were used to analyze expected concentration in Flood-1. In the context of our experimental design, where flood water with low solute concentration (Table S2) was mixed with groundwater with high solute concentration, the potential reactive solutes would be expected to be diluted, if no reaction occurred (Paradis et al., 2020). Thus, the breakthrough curves of a solute are bound by the flood water in the lower concentrations and groundwater in the upper concentrations; with the expected concentrations being between the two boundaries. The expected concentrations are based on the behavior of added non-reactive tracers, namely bromide for Flood-1 and iodide for Flood-2. The expected concentration assumes that the solutes in groundwater would behave as added non-reactive tracers and thus only be dominated by advection and dispersion during floodings (Paradis et al., 2019). When plotted on the same graph, any difference between observed and expected breakthrough curve will indicate reactivity of the solute. For an evaluation of solutes being added or removed from the groundwater, an observed concentration greater than the expected concentration indicates constituent addition, and vice versa (Paradis et al., 2020). The expected concentrations were determined using Eq. (11) from Paradis et al. (2019). The equation generates the expected concentration of a potentially reactive solute due to dilution occurred upon mixture of low concentration flood water and high concentration aquifer fluids. More detailed derivation and parameters of the expected concentration equation and its assumptions can be found in Paradis et al. (2019).

While the above-mentioned approach is a qualitative measure of reactivity, a quantitative measurement of reactivity and subsequent mechanisms was done using relative temporal moment analysis (TMA) (Paradis and Sultana, 2024). The principle of relative TMA is to evaluate the behavior of solutes in a system by analyzing their temporal distribution; all without the need to solve the advection-dispersion-reaction equation or modify true concentrations. This relative approach involved calculating the ratio of observed to expected zeroth temporal moments, the ratio of observed to expected normalized first temporal moments, and the ratio of observed to expected normalized second temporal moments via Eqs. (21), (22), and (23), in Paradis and Sultana, 2024. The zeroth moment measures the area underneath the breakthrough curve. The normalized first moment is the first moment divided by the zeroth moment and indicates the center of mass in time [T]. Likewise, the normalized second moment is the second moment divided by the zeroth moment and represents the spread in time squared [$T^2$]. Finally, the ratio calculations resulted in unitless and dimensionless temporal moments, which are relative zeroth moment ($M_o$), relative first moment ($M_1$) and relative second moment ($M_2$). More detailed derivation and parameters of the relative moment equations can be found in Paradis and Sultana (2024).

$M_o$,$M_1$, and $M_2$ were applied to calculate the mass, advection and dispersion, respectively for all potential reactive solutes and added tracers. $M_o > 1$ indicates a net addition of solute mass to the aqueous phase, whereas $M_o < 1$ indicates a net removal; $M_o = 1$ indicates no net addition or removal. Similarly, $M_1 \neq 1$ indicates a change in solute advection and $M_2 \neq 1$ indicates a change in solute dispersion. The overall reactivity of a reactive solute, reactivity index (RI), can be quantified by calculating the weighted residual sum of squares for each of the three relative moments from Eq. (24) in Paradis and Sultana, 2024. In theory, RI = 0 indicates no reactivity whereas RI > 0 indicates reactivity; negative RI values of RI is not viable. Equal moment weights for mass, advection, and dispersion ($\omega_0 = \omega_1 = \omega_2 = 1$), and a multiplication factor (f) of 1000 were applied. The weights ($\omega$i) and multiplication factor (f) in Eq. (24) are chosen by the user. The weights ($\omega$i) can vary depending on how much weight to put on reactions that affect mass ($M_o$), advection (M1), and dispersion (M2). The multiplication factor (f) can typically be some factor of 10, e.g., 10, 100, 1000, etc., to avoid decimals and ensure whole numbers which are easier to comprehend, making negative values of the multiplication factor not viable. However, it is important to consider the relative reactivity

among $k^{th}$ solutes while approximate these numerical approaches.

#### 2.3.2. Mass calculation

Transect-wise mass calculation was completed for reactive solutes (U, Cl, $SO_4$, Na, Mg, K, Ca, Mn, Mo) and tracers (Br and I). Due to being below the detection limits (0.03 mg/L), transect-wise mass for $Fe^{2+}$ could not be calculated. The total Fe ($Fe^{2+}$+$Fe^{3+}$) data was also not considered due to its noisy signals. Thus, considering $Fe^{2+}$ or total Fe data for the mass calculation was of limited usefulness. For other reactive solutes, both observed and expected mass going through a transect was calculated. Among the three transects (Fig. 2), Transect-2 had the maximum number of wells with substantial signals from the tracers during our study. Thus, in this study, the mass calculation will be discussed for transect-2. It is to be noted that, well no. 1007 was excluded while calculating transect wise mass since it did not have any detectable tracer signal. The mass of solutes going through transect-2 was determined in two steps. First, the Theissen Polygon Method (TPM) (Mackay et al., 2012) was used to calculate the mass discharge of the solutes going through transect-2. The density (1.08 points/$m^2$) and the distance between the wells (average 0.08 m) in transect-2 were in agreement (Mackay et al., 2012) to ensure TPM calculation accuracy. In the TPM calculation at our site, while the concentration varied in each scenario, the hydraulic conductivity (1.8 m/day) and hydraulic gradient (0.03) were assumed constant. The hydraulic conductivity was calculated based on groundwater velocity (0.18 m/day) at the site (Paradis et al., 2022b), hydraulic gradient (0.03) and porosity (0.3) of the sandy groundwater. Finally, the mass of each solute was determined by calculating the area under the breakthrough curve of the calculated mass discharge of the respective solutes. The time duration (40 days) was kept constant, and the mass discharge was kept similar for each solute in both the experiments. An analytical error of 10% was applied to all the calculated values. The percentage was selected as it aligns with standard practices in similar studies (Paradis et al., 2022a), where a 10% margin is commonly accepted as reasonable.

#### 2.3.3. Spatial analyses

The contoured maps for both observed and expected solute concentrations were constructed using the anisotropic kriging interpolation method in Surfer version 24 (Surfer® from Golden Software, LLC, www.goldensoftware.com). Due to the skewed distribution of tracer and chloride concentration data, the concentrations were log transformed prior to creating the grid file in Surfer (Ricker, 2008) and then inverse log transformed before plotting. The center mass of the tracer plumes was calculated (Ricker, 2008) and plotted after filtering data to include concentrations greater than approximately 10% of the initial concentration added with flood water.

All the data processing and analyses were performed using Microsoft Excel 2016 and Python (version 3.11.3).

## 3. Results and discussions

The experimental results and their interpretations are presented in the following sections that start with (1) plume distribution maps of added tracers, uranium and chloride in the experimental location (Section 3.1.1), (2) observed and expected breakthrough curves of chloride (Section 3.1.2), and uranium and sulfate (Section 3.1.3), along with transect-wise mass calculation of non-reactive added tracers and potentially reactive solutes (U, Cl, $SO_4$, Na, Mg, K, Ca, Mn, and Mo) (Section 3.1.3), (3) identifying hydrogeological compartment that is responsible for mobilization of solutes (Section 3.2), (4) mobilization mechanisms with moment analyses, M (zeroth moments, relative first and relative second moments) with reactivity indices (RI) (Section 3.3 with results from the two flooding experiments summarized in Table 2), and (5) evaluating the impact of added alkalinity as a remediation effort (Section 3.4). Finally, our experimental data were combined with previous solid-phase data on evaporites (U.S. Department of Energy, L.M, 2014), and direct injection experimental data (Paradis et al., 2022a) to support possible contaminant mobilizing and mechanistic insights.

### 3.1. Mass mobilization of solutes

#### 3.1.1. Plume distribution maps of added tracers, uranium, and chloride

During Flood-1, the flood water contained bromide as an added tracer and infiltrated for about 8 days (Table 1) through the flood basin (Fig. 2). The center of mass of the resulting plume moved in a south-east (SE) direction, with notable concentrations detected in monitoring wells 1001, 1005, and 1011 post flooding (Fig. 3a). Tracer mass calculations revealed that about 23% (218 g) of the total bromide mass (949 g) passed (Fig. S5) across transect-2 (Fig. 2) during the flooding, with higher masses observed in wells 1001, 1005, and 1011 (Fig. S6). Bromide isocontours illustrated a relatively consistent distribution of the flood water which is evident in both spatial (Fig. 3a) and temporal (Fig. S3) patterns. The spatial and temporal extent with elevated signals across the three transects of the well gallery (Fig. 3a) implied that a significant volume of flood water traversed the experimental site during the experiment.

Before Flood-1, uranium exhibited a uniform distribution, with concentrations ranging from 0.88 to 1.12 mg/L in the groundwater (Fig. 3b). However, following the flooding, uranium concentrations increased, ranging from 0.89 to 1.51 mg/L on day 15 (Fig. 3c). The flood water had a negligible uranium concentration (0.01 mg/L) than the groundwater uranium concentration (mean = 0.97 mg/L). Consequently, the observed uranium concentration would be expected to be diluted, ranging from 0.41 to 1.09 mg/L (Fig. 3d). Instead of being diluted as expected, higher uranium concentrations were detected along the path of the flood water, suggesting significant uranium mobilization during the flooding, eventually entering the groundwater (Fig. 3e). The distribution and direction of the added uranium in the groundwater corresponded to that of bromide, indicating uranium addition during the

**Table 2**
Temporal moment analysis (M) of chloride (Cl), uranium (U), and sulfate ($SO_4$) showing relative zeroth, relative first ($M_1$) and relative second moment, about the mean ($M_2$) with Reactivity Indices (RI).

| | M | Well 1001 | | | Well 1005 | | | Well 1011 | | |
|---|---|---|---|---|---|---|---|---|---|---|
| | | Cl | U | $SO_4$ | Cl | U | $SO_4$ | Cl | U | $SO_4$ |
| Flood-1 | $M_o$ | 1.26 | 1.25 | 1.26 | 1.52 | 1.66 | 1.54 | 1.25 | 1.40 | 1.34 |
| | $M_1$ | 0.91 | 0.92 | 0.91 | 0.96 | 0.96 | 0.95 | 1.03 | 1.03 | 1.04 |
| | $M_2$ | 0.87 | 0.87 | 0.87 | 0.82 | 0.81 | 0.82 | 0.84 | 0.80 | 0.80 |
| | RI | 9.13 | 8.23 | 9.39 | 29.9 | 47.81 | 32.87 | 8.86 | 20.10 | 15.47 |
| | M | Well 1000 | | | Well 1005 | | | Well 1010 | | |
| | | Cl | U | $SO_4$ | Cl | U | $SO_4$ | Cl | U | $SO_4$ |
| Flood-2 | $M_o$ | 1.09 | 1.42 | 1.45 | 1.11 | 1.40 | 1.35 | 1.04 | 1.39 | 1.31 |
| | $M_1$ | 1.00 | 0.93 | 0.93 | 0.99 | 0.96 | 0.98 | 1.00 | 1.12 | 1.11 |
| | $M_2$ | 0.97 | 0.86 | 0.85 | 0.99 | 0.86 | 0.88 | 0.98 | 0.91 | 0.95 |
| | RI | 1.02 | 20.09 | 23.19 | 1.16 | 18.21 | 13.96 | 0.17 | 18.13 | 10.89 |

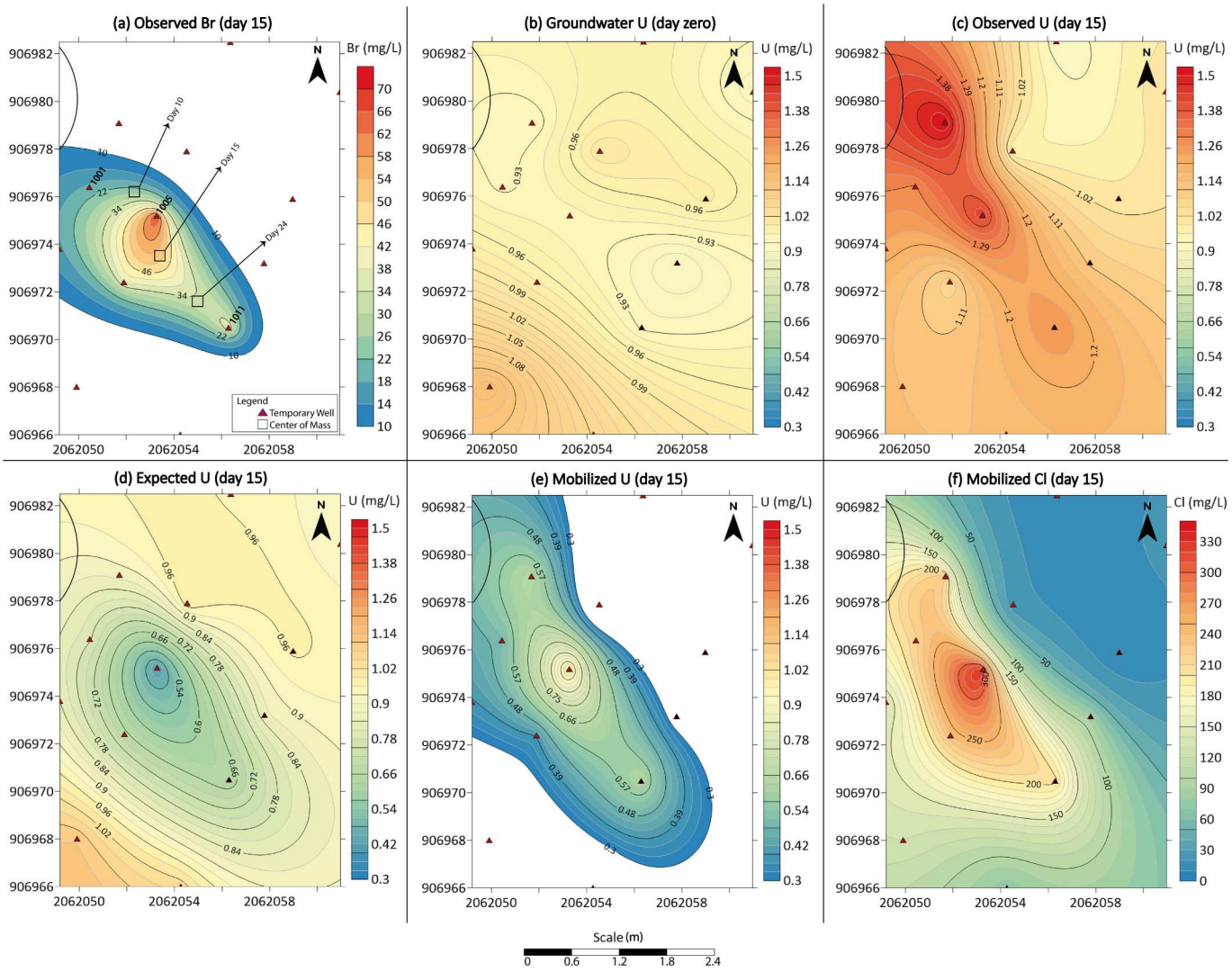


**Fig. 3.** ***Flood-1:*** (a) Homogenous bromide (Br) isocontours after flooding, (b) homogeneous uranium (U) distribution before flooding, (c) elevated observed uranium concentration after flooding, (d) diluted expected uranium (U) after flooding, (e) mobilized uranium (U) during flooding, (f) mobilized chloride (Cl) during flooding. It is noteworthy that uranium (0.01 mg/L) and chloride (14 mg/L) concentrations were very low in flood water compared to that of groundwater (uranium = 0.97 mg/L and chloride = 422 mg/L). The semi-circle at the upper left of each figure indicates the location of the flood basin. The plume maps are skewed to SE direction, in line with groundwater flow direction.

flooding. Additionally, chloride exhibited a similar pattern to uranium, further suggesting mobilization of potentially reactive solutes during the flooding event (Fig. 3f).

During Flood-2, the flood water contained iodide as an added tracer and infiltrated for about 12 days (Table 1) through the flood basin (Fig. 2). The center of mass of the resulting plume followed a southeast direction, with elevated iodide signals detected in monitoring wells 1000, 1005, and 1010 post flooding (Fig. 4a). Tracer mass calculations revealed that about 28.3% (600 g) of the total infiltrated iodide mass (2118 g) passed across transect-2 (Fig. 2) during Flood-2 (Fig. S5), with higher masses observed in wells 1000, 1005, and 1010 (Fig. S6). Unlike bromide in Flood-1, iodide isocontours illustrated a heterogeneous behavior across the site in Flood-2 (Fig. 4a). The heterogeneity was also evident in the breakthrough curve patterns with double hump pattern in the breakthrough curves (Fig. S3). Despite the heterogeneity observed during Flood-2, the spatial (Fig. 4a) and temporal (Fig. S3) extent of iodide with elevated signals across the three transects of the well gallery suggested that a significant volume of flood water passed through the experimental site.

Before Flood-2, uranium concentration in groundwater ranged from 0.84 to 1.08 mg/L with a homogenous distribution in the groundwater (Fig. 4b). The data indicated that aqueous uranium concentration reached a similar range as the first flooding (Flood-1) before initiation of Flood-2. Following the initiation of Flood-2, the aqueous uranium concentration increased, ranging from 0.85 to 1.41 mg/L with higher values being concentrated along the flood water path (Fig. 4c). Similar to Flood-1, flood water during Flood-2 had a lower uranium concentration (0.01 mg/L) than that of groundwater (mean = 0.94 mg/L). Consequently, the uranium concentration in the groundwater after the experiment would be expected to be diluted, ranging from 0.34 to 1.06 mg/L (Fig. 4d). However, the observed uranium concentration did not behave as expected, indicating a substantial amount of uranium was mobilized and added (Fig. 4e) to the groundwater during the experiment. The plume pattern and direction of the mobilized uranium in the groundwater corresponded to that of iodide, indicating uranium was mobilized and added during the flooding. Furthermore, chloride was also observed to be mobilized in a similar pattern to uranium (Fig. 4f). While much lower chloride mobilized during Flood-2 compared to Flood-1, the area of higher concentration of the chloride plume corresponded to that of iodide and uranium, indicating that the chloride was

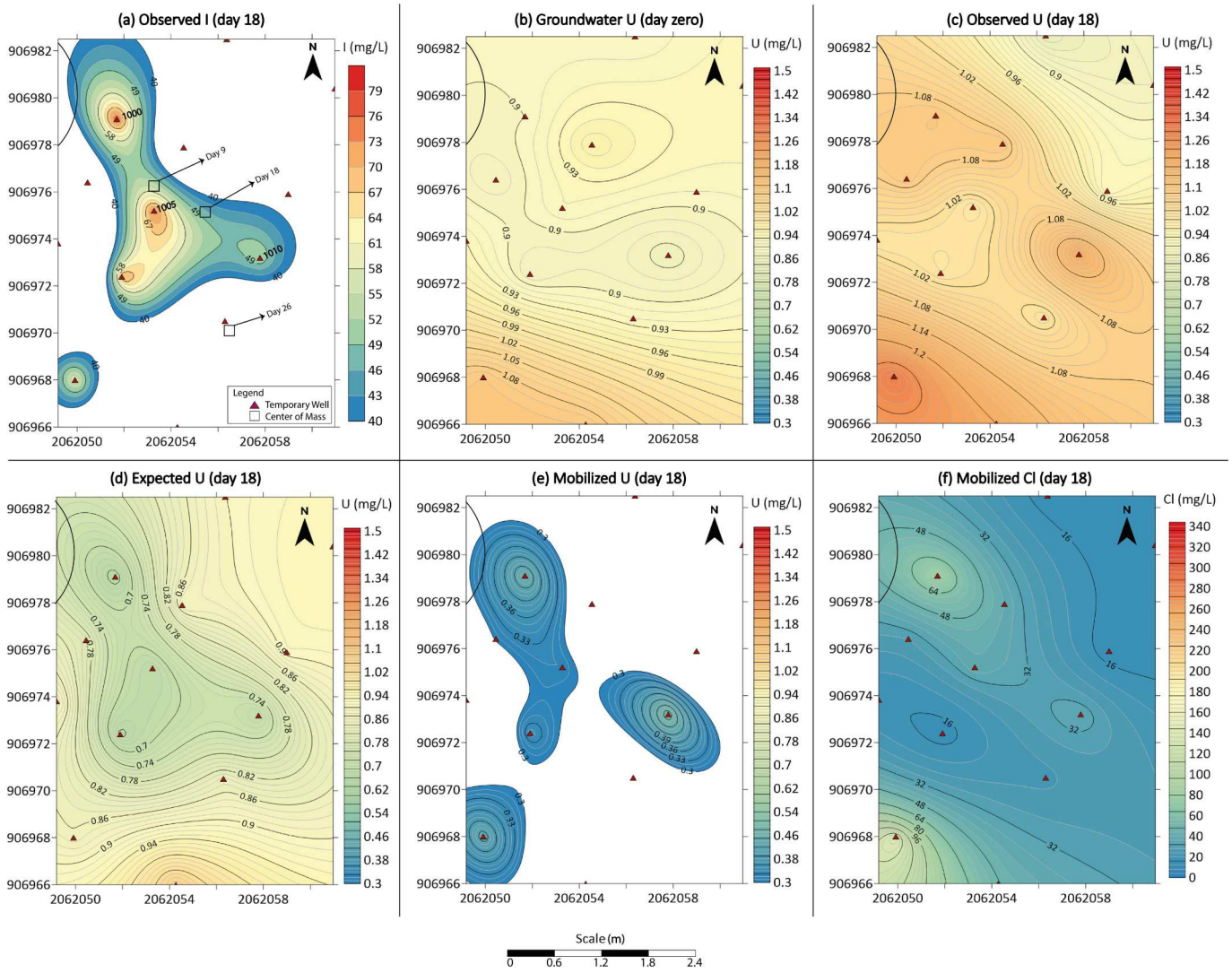


**Fig. 4.** ***Flood-2:*** (a) Heterogenous iodide (I) isocontours after flooding, (b) homogeneous uranium (U) distribution before flooding, (c) elevated observed uranium concentration after flooding, (d) diluted expected uranium (U) after flooding, (e) mobilized uranium (U) during flooding, (f) mobilized chloride (Cl) during flooding. It is noteworthy that uranium (0.01 mg/L) and chloride (66 mg/L) concentrations were very low in flood water compared to that of groundwater (uranium = 0.94 mg/L and chloride = 328 mg/L). The semi-circle at the upper left of each Fig. indicates the location of the flood basin. The plume maps are skewed to SE direction, in line with groundwater flow direction.

mobilized during Flood-2. These results reinforced the concept of contaminant mobilization during flooding events.

### 3.1.2. *Chloride breakthrough curves*

During Flood-1, the signal of the observed breakthrough curve was notably stronger at well 1001, gradually decreasing in wells 1005 and 1011. However, the observed and expected breakthrough curves of chloride differed across the transects during Flood-1 (Fig. 5). These results suggested that mass transport characteristic of chloride was different than that of added tracer (bromide) and chloride mobilization was controlled by mechanisms other than advection and dispersion during the flooding (Paradis et al., 2019). Furthermore, observed chloride concentrations exceeded expected concentrations in all three wells (Fig. 5). The results indicated a net addition of chloride in the groundwater during the flooding event (Paradis et al., 2019) that resulted in approximately 29% chloride mass increase in groundwater (Fig. 8).

During Flood-2, the signal of the observed breakthrough curve was relatively stronger at well 1000, gradually decreasing in wells 1005 and 1010. Similar to Flood-1, the observed and expected breakthrough curves of chloride were not identical throughout the transects during Flood-2 (Fig. 5). Consistent to results obtained in Flood-1, these observations indicated that mobility of chloride differed from than that of added tracer (iodide) and the mobility was controlled by mechanisms other than advection and dispersion during the flooding (Paradis et al., 2019). Additionally, Fig. 5 indicated that after approximately 5 days, the observed breakthrough curves of chloride aligned closely with expectations, suggesting dilution occurred after this period during Flood-2. Moreover, the observed chloride concentrations did not substantially exceed the expected concentrations, as seen in Flood-1 in all three wells (Fig. 5). The results indicated that despite a net addition of chloride resulting in about 10% chloride mass increase in groundwater (Fig. 7), there was a considerable decline in chloride mass during Flood-2 compared to Flood-1.

### 3.1.3. *Uranium and sulfate breakthrough curves*

The signal of the observed breakthrough curve was relatively stronger at well 1001, gradually decreasing in wells 1005 and 1011 for both contaminant species (uranium and sulfate) (Fig. 6 and Fig. 7). The observed and expected breakthrough curves of the contaminants were not identical throughout the transects during Flood-1 (Fig. 6 and Fig. 7).

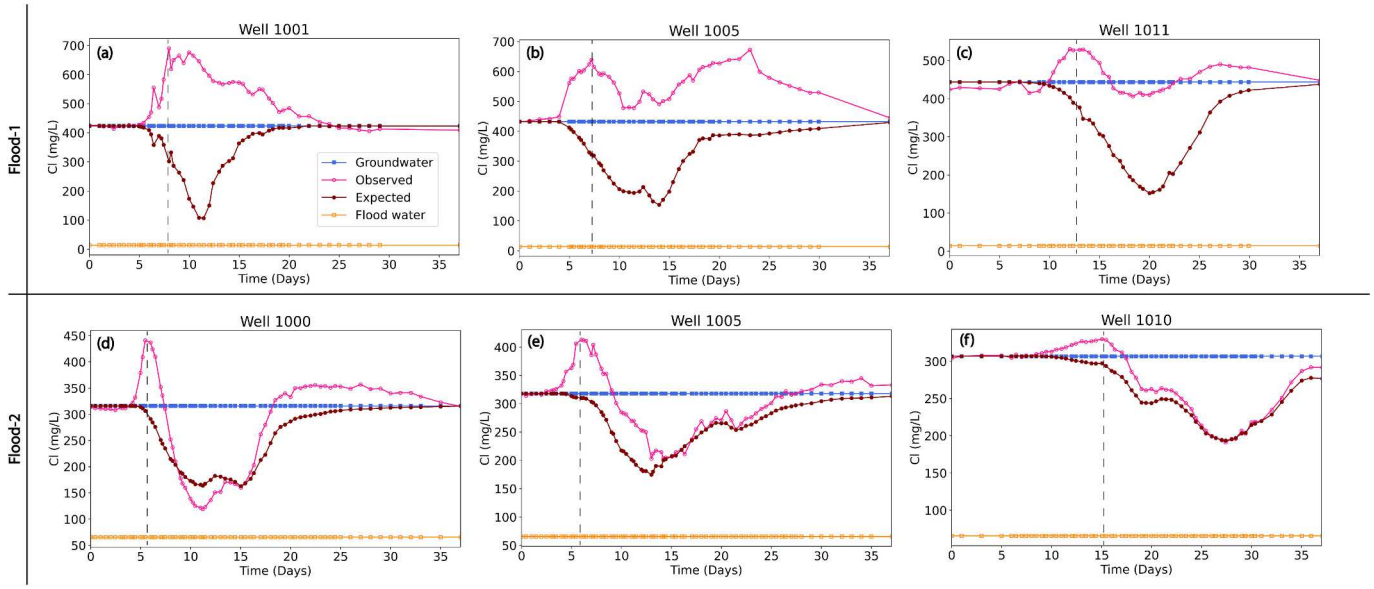


**Fig. 5.** Chloride breakthrough curves in (a) well 1001 (transect-1), (b) well 1005 (transect-2), and (c) well 1011 (transect-3) during Flood-1; (d) well 1000 (transect-1), (e) well 1005 (transect-2), and (f) well 1010 (transect-3) during Flood-2. The dashed line shows the arrival times of the maximum concentrations of the 'observed' breakthrough curves.

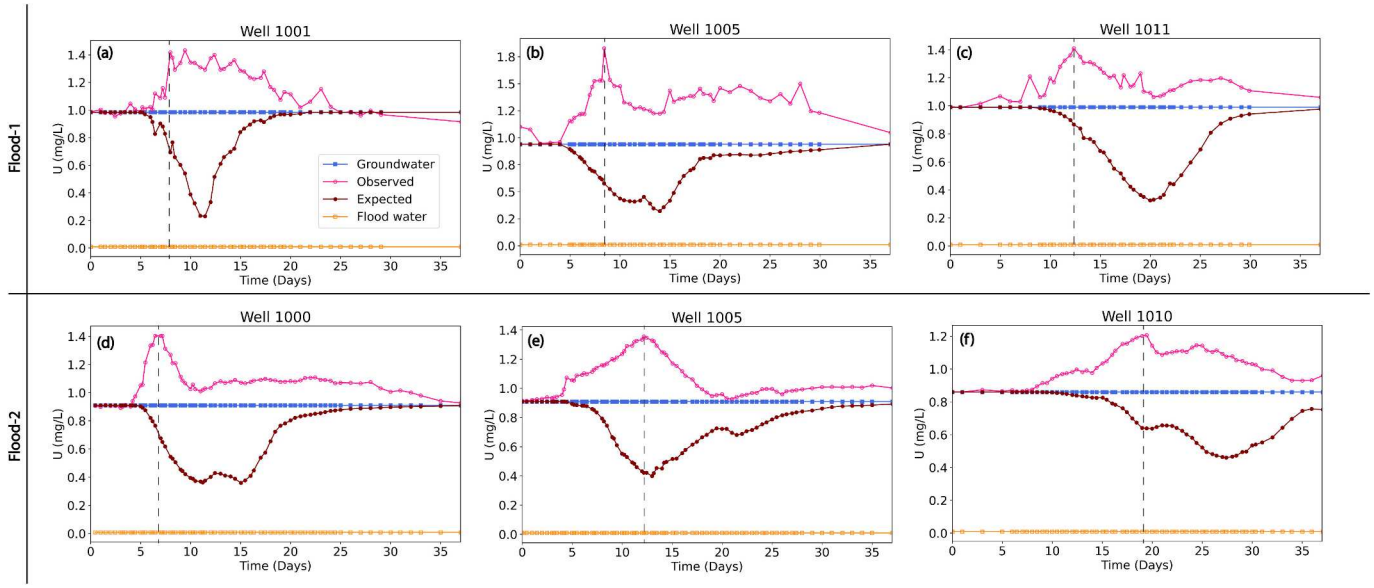


**Fig. 6.** Uranium breakthrough curves in (a) well 1001 (transect-1), (b) well 1005 (transect-2), and (c) well 1011 (transect-3) during Flood-1; (d) well 1000 (transect-1), (e) well 1005 (transect-2), and (f) well 1010 (transect-3) during Flood-2. The dashed line shows the arrival times of the maximum concentrations of the 'observed' breakthrough curves.

These results suggested that the mobility of the contaminants during Flood-1 was dissimilar to that of the added tracer (bromide), indicating that other mechanisms beyond advection and dispersion controlled their mobility during the flooding event (Paradis et al., 2019). Moreover, the breakthrough curves of observed uranium and sulfate concentrations exceeded the expected curves during the event (Fig. 6 and Fig. 7), indicating a net addition of the contaminants (Paradis et al., 2019). The net addition resulted in approximately 21% of uranium and 24% of sulfate mass increase in groundwater (Fig. 8).

Similar to Flood-1, the observed and expected breakthrough curves of the contaminants (uranium and sulfate) differed from each other in all three wells during Flood-2 (Fig. 6 and Fig. 7). These results indicated that the mobilization of uranium and sulfate was different than that of added tracer (iodide), and the mobility was controlled by mechanisms other than advection and dispersion during the flooding (Paradis et al., 2019). Similar to Flood-1, the observed uranium concentration exceeded significantly than expected concentrations during Flood-2. The results indicated a net addition of contaminants which caused about 24% of uranium and 25% of sulfate mass increase (Fig. 8) in groundwater during Flood-2.

Similar to chloride, uranium, and sulfate, the mobilization of other potentially reactive solutes (Na, Mg, K, Ca, Mo) differed from that of the added tracers during flooding events, indicating a net addition to the groundwater (Fig. 8). However, a substantial reduction in manganese mass was observed during both flooding events (Fig. 8). Other redox sensitive ion, iron ($Fe^{2+}$) revealed a notably low concentration of 0.42

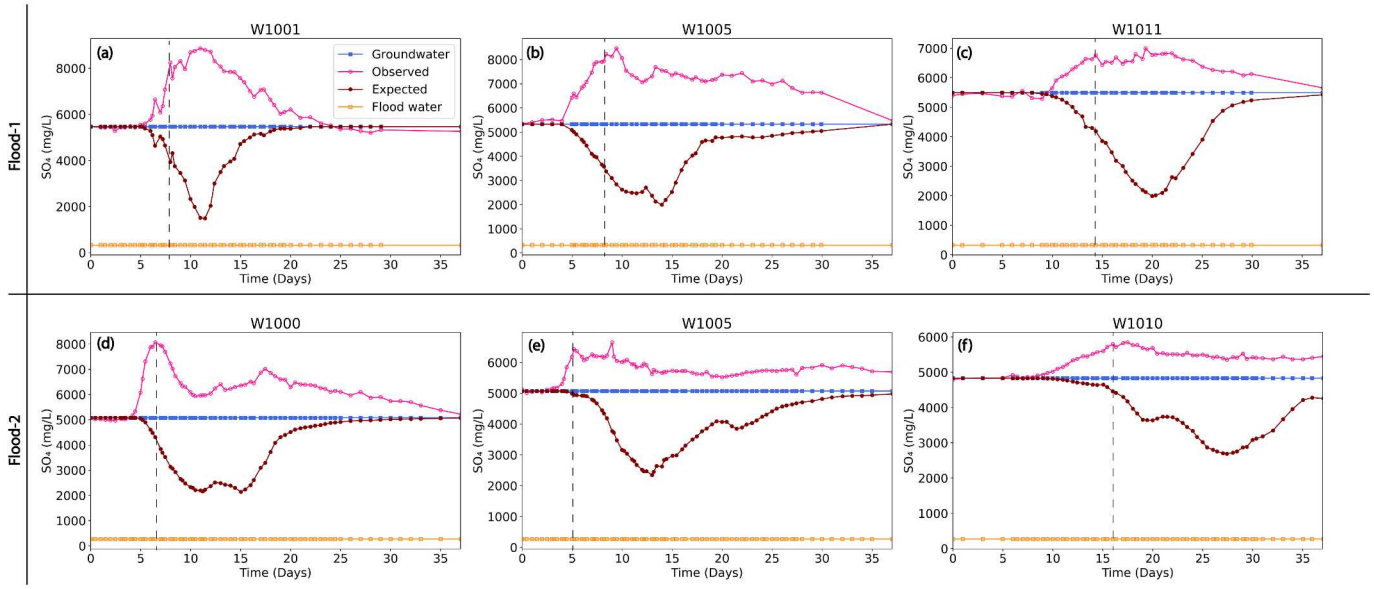


**Fig. 7.** Sulfate breakthrough curves in (a) well 1001 (transect-1), (b) well 1005 (transect-2), and (c) well 1011 (transect-3) during Flood-1; (d) well 1000 (transect-1), (e) well 1005 (transect-2), and (f) well 1010 (transect-3) during Flood-2. The dashed line shows the arrival times of the maximum concentrations of the 'observed' breakthrough curves.

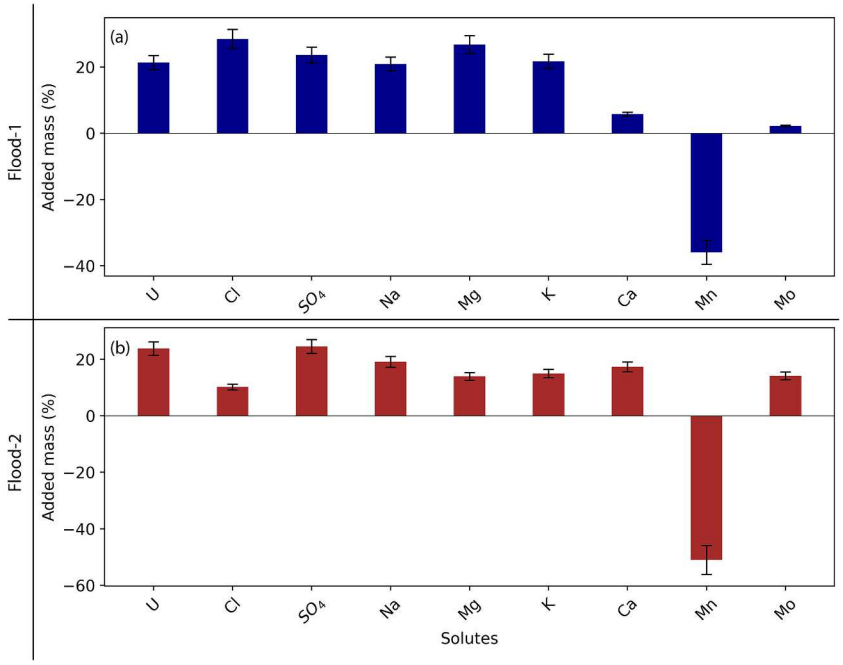


**Fig. 8.** Added (U, Cl, $SO_4$, Na, Mg, K, Ca, Mo) and removed (Mn) of potentially reactive solutes during (a) Flood-1 and (b) Flood-2 in transect-2.

mg/L in well 1001 (Fig. 2), which gradually decreased below detection limit of 0.03 mg/L along the transects during both flooding experiments. It is possible that the flooding of oxygenated river water (ORP = 103 mV in Flood-1 and ORP = 207 mV in Flood-2) caused manganese and iron ($Fe^{2+}$) to eventually precipitate or get adsorbed within sediments (Aiken and Ying, 2023; Singh et al., 2014).

### 3.2. Mobilizing hydrogeological compartment

Our study area is characterized by two compartments (Fig. 9) which are an overlying vadose zone and an underlying groundwater (Dam et al., 2015). The injection experiment (mentioned in Section 2.1), conducted directly into the aquifer prior to our flooding experiments, found that the potentially reactive solutes (chloride, uranium, sulfate, sodium, magnesium, potassium, calcium, and molybdenum) behaved conservatively as expected, except for manganese and iron in the aquifer (Paradis et al., 2022a). The study concluded that these reactive solutes (except for manganese and iron) in the aquifer sediments were non-reactive and did not get mobilized upon direct injection to the groundwater. In contrast, during our flooding experiments, where the flood water travelled through the vadose zone (Fig. 9) before entering the groundwater, mobilization of reactive solutes and the addition of the solute mass to the groundwater were observed (Fig. 8). The results from our study suggested that while manganese and iron decreased their

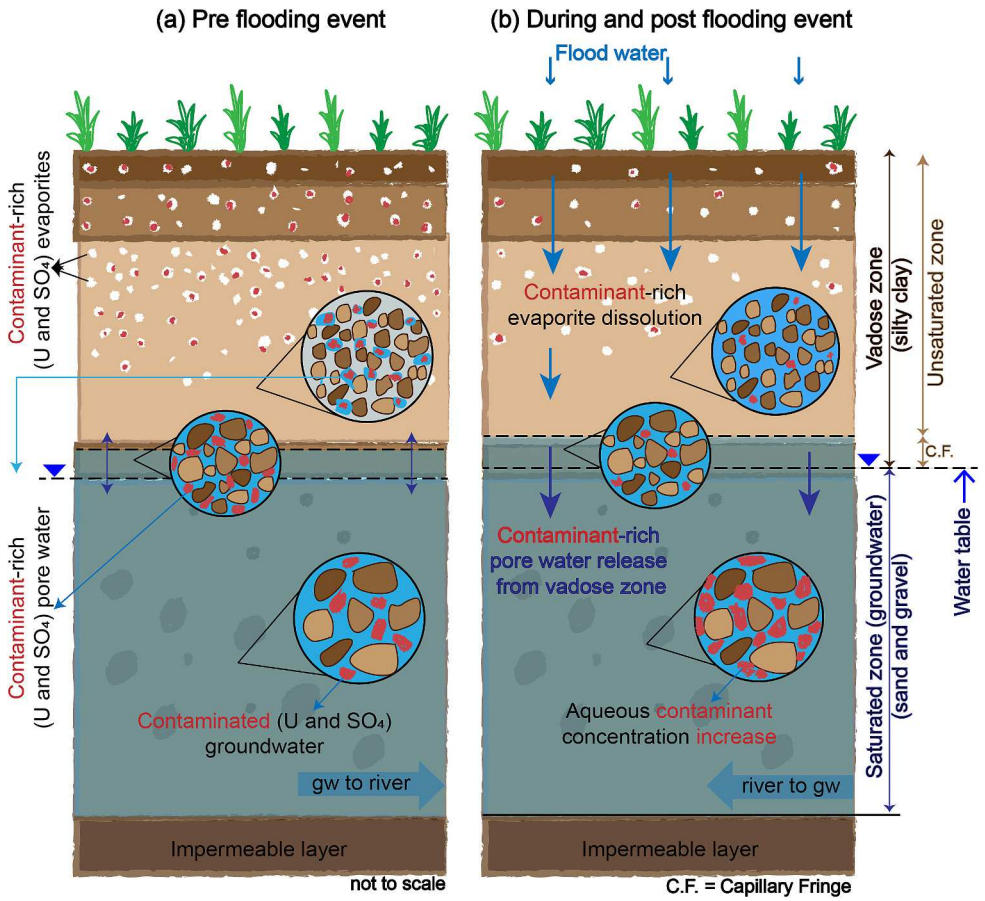


**Fig. 9.** Conceptual figure of the hydrogeological compartments and mobilization mechanism of the contaminants (uranium and sulfate) (a) pre flooding evens and (b) during and post flooding events; the blue arrows show downward infiltration. The red dots represent contaminants in solid-phase evaporites, vadose zone pore water and groundwater. (For interpretation of the references to colour in this figure legend, the reader is referred to the web version of this article.)

mobility during the floodings, all other potentially reactive solutes, exhibited reactivity and increase mobilization, resulting in a substantial release of these solutes into the groundwater during the flooding experiments (Fig. 8). The contrast between the findings of the previous study (Paradis et al., 2022a) and our analyses indicated that mass mobilization during the flooding experiments occurred primarily from the vadose zone and not from the aquifer. The results are in line with the three-year multilevel groundwater monitoring data report at our study site, Riverton (U.S. Department of Energy, 2019). The report showed that the concentration of the reactive solutes in shallow groundwater increased during large flooding events in 2010, 2016 and 2017, near the Little Wind River (Fig. S1). However, the groundwater quality remained unchanged during monitoring in 2018 when no flooding or extreme recharge events occurred. The results from our study and well monitoring indicated that vadose zone is the key hydrogeological compartment that served as a storage for contaminants before the flooding events and that the contaminants were substantially mobilized from the vadose zone during the events.

### 3.3. Mobilization mechanisms

#### 3.3.1. Physical mobilization

During Flood-1, the observed breakthrough curves of the contaminants (uranium, and sulfate) along with chloride exhibited a gradual arrival of a peak throughout the transects (Fig. 5, Fig. 6, and Fig. 7). The arrival of the peak of observed chloride, uranium and sulfate breakthrough curves was approximately 4 days earlier in well 1001, and about 3 days earlier in well 1005 and about 7 days earlier in well 1011 than that of expected (Fig. 5, Fig. 6, and Fig. 7). These data suggested that chloride, sulfate, and uranium arrived earlier than the tracer-induced flood water during Flood-1.

During Flood-2, the observed breakthrough curves of contaminants (uranium, and sulfate) along with chloride exhibited a rapid arrival of a peak in well 1000. The peak concentration became gradually less pronounced in wells 1005, and 1010 (Fig. 5, Fig. 6, and Fig. 7). The peak of observed chloride concentrations arrived about 6 days earlier in well 1000, 7 days earlier in well 1005, and 3 days earlier in well 1010 than that of expected (Fig. 5). The peak of observed uranium concentrations arrived about 4 days earlier in well 1000, about 1 day earlier in well 1005 than that of expected, and almost at the same time as the expected in well 1010 (Fig. 6). The peak of observed sulfate concentrations arrived about 4 days earlier in well 1000, 7 days earlier in well 1005, and 2 days earlier in well 1010 than that of expected (Fig. 7). These data suggested that chloride, uranium, and sulfate arrived earlier than the tracer-induced flood water during Flood-2.

The early arrival of the peak concentrations during both floods can be explained by the action of a compression wave that propagate through saturating density-driven fluid (Gross et al., 2003). During a flooding event, the arrival of flood water at the surface causes an abrupt pressure change, that subsequently generates the compression wave. Such abrupt pressure changes often occur at the wetting fronts of floodings (Amiaz et al., 2011; Dahan et al., 2008). In our flooding experiments, the wetting fronts were indicated by the arrival of the non-reactive tracers in the expected breakthrough curves (Fig. 5, Fig. 6, and Fig. 7). The compression wave, in turn, enhances the advection of solute and can cause abrupt solute-displacement in the groundwater (Amiaz et al., 2011). The mechanisms are also suggested by mathematical models developed for compressible fluid (Sorek and Bear, 1990)

and compressible fluid with a solute in saturated porous media, following the onset of an abrupt pressure change (Sorek, 1996). These mechanisms can be attributed to wave-driven transport, regardless of saturated or unsaturated conditions (Amiaz et al., 2011). Moreover, Warrick et al., 1971 theoretically and experimentally showed solute displacement in the vadose zone with percolating water where the displacement is highly dependent on the moisture content at the soil surface during infiltration.

In view of the previous studies, the results from our study suggested that contaminant-rich pore water in the vadose zone (Fig. 9) could be impacted by the propagating wave, thereby generating the peak ahead of the tracer-induced flood water. In addition, the pore water can accumulate a significant amount of contaminants that become more concentrated in the variably saturated zone and gradually dilutes closer to the water table (Du Laing et al., 2007; Nativ et al., 1995). Therefore, in our flooding experiments, it is plausible that the tracer-induced flood water generated the compression wave upon arrival the surface and subsequently propelled solute-concentrated pore water above the water table (Fig. 9) and then into the groundwater, leading to the earlier arrival of the solute pool.

### 3.3.2. *Chemical mobilization*

During Flood-1, the breakthrough curves of chloride, uranium, and sulfate (Fig. 5, Fig. 6, and Fig. 7) showed a sustained elevated concentration for the duration of the flooding. The data suggested that an additional mobilization mechanism was prominent for all three solutes during the flooding event. The reactive mobilization was further quantified via relative temporal moment analysis (Paradis and Sultana, 2024) of the solute breakthrough curves. These relative moments (M) characterize mass ($M_o$), advection ($M_1$), and dispersion ($M_2$) of a solute with numeric values. The numerical values indicate the dominant mobilization mechanism of a solute and measure its reactivity with reactivity index (RI). In addition, such values identify solutes with similar transport mechanisms to further understand their potential mechanisms of reactive transport.

Analysis of the relative moments for bromide, a non-reactive tracer, yielded expected results, with its relative moments (M) equal to one and a reactivity index (RI) of zero, indicating no reactivity throughout the transects (Table S4). However, for the reactive solutes, $M_o$ were significantly >1, with $M_1$ and $M_2$ moments were closer to 1 and RI greater than zero (Table 2). The RI values suggested reactivity of the solutes that is attributed to their reactive mass mobilization based on $M_o$ values, during Flood-1. These findings align with breakthrough curve observations and the added mass of the solutes (Fig. 8). In addition, the values of $M_o$, $M_1$ and $M_2$ of chloride, uranium, and sulfate were almost similar throughout the transects with reactivity indices closer in values in well 1001 than others (Table 2). The data suggested that the additional mass mobilization mechanism for chloride and the contaminants (uranium and sulfate) were similar to each other during the flooding event.

During Flood-2, the breakthrough curves of uranium and sulfate (Fig. 6 and Fig. 7) consistently exhibited elevated concentrations throughout the flooding period. In contrast, the sustained elevated concentration of chloride was negligible after its initial peak arrival (Fig. 5). The difference suggested that while an additional mobilization mechanism was prominent for uranium and sulfate during Flood-2, it was not significant for chloride. The reactive mobilization was further quantified via moment calculation (Paradis and Sultana, 2024) of the solute breakthrough curves. Iodide, a non-reactive tracer, exhibited relative moments (M) equal to one and a reactivity index (RI) of zero in all three wells, as expected (Table S3). In contrast, for uranium and sulfate, the relative moments $M_o$ was significantly >1, while the relative $M_1$ and $M_2$ moments were closer to 1 with reactivity indices significantly greater than zero (Table 2). The results of RI indicated reactivity of the contaminants (uranium and sulfate) that could be attributed to their reactive mass mobilization based on the $M_o$ values, during Flood-2. These results are consistent with the breakthrough curve observations and the added mass of the solutes (Fig. 8). In contrast, chloride exhibited relative moments, $M_o$ that was not significantly >1, and $M_1$ and $M_2$ closer to 1 with RI significantly closer to zero (Table 2). The results of RI indicated that, unlike Flood-1, chloride was not significantly reactive during Flood-2, which was also evident in the breakthrough curves of chloride (Fig. 4). In addition, the values of $M_o$, $M_1$, $M_2$ and RI for the contaminants were almost similar throughout the transects, whereas these values for chloride was significantly different from that of contaminants. The results suggested that, while the additional mass mobilization mechanism for contaminants was similar during Flood-2, chloride behaved differently.

The additional mass mobilization mechanism during Flood-1 for chloride, uranium, and sulfate, and during Flood-2 for uranium and sulfate, can be explained by the generation of wetting fronts by flood water propagating downward through the vadose zone to the water table (Fig. 9) during flooding events (Dahan et al., 2008). During the dry seasons the sediments in the vadose zone accumulate high concentration evaporite salts (Fig. 9) due to evaporation of sediment pore water to a low water content (Amiaz et al., 2011). As recharge proceeds during the flooding events, percolating flood water through the vadose zone interacts with soluble salts and the flood water wetting front leaches out salts (Fig. 9) from the vadose zone (Amiaz et al., 2011). The evaporite salts, notably bearing chloride and sulfate, are highly soluble when in contact with water (Drever, 1982). Surface and subsurface evaporites with concentrated uranium were also observed in our study area (Johnson et al., 2016). The majority of these evaporites were sulfate- and chloride-bearing evaporites (U.S. Department of Energy, 2019) where sulfate was present at an average of 85 g/kg with uranium concentrated at an average of 0.014 g/kg (U.S. Department of Energy, L. M, 2014). Therefore, it is possible that as the wetting front of the flood water was propagating during our flooding experiments through the vadose zone, it dissolved the precipitated sulfate- and chloride-bearing evaporites with concentrated uranium and subsequently released then into groundwater. The relative moments analysis and solid-phase data suggested that the additional mass mobilization was prominently via uranium-rich sulfate evaporite dissolution likely forming uranium-bearing evaporite couple such as $U(SO_4)_2$, $UO_2SO_4$, $UO_2(SO_4)_2^{2-}$, as identified from PHREEQC simulations, during both flooding events. Contaminant release from the evaporite dissolution was further supported by the release of other evaporite-related constituents (sodium, calcium, magnesium, and potassium) from the vadose zone during both flooding events (Fig. 8), which were likely in sulfate-bearing evaporite forms ($NaSO_4^-$, $CaSO_4$, $MgSO_4$, and $KSO_4^-$). The release of the evaporite-related constituents with uranium were also observed during larger flooding events occurred in 2016 and 2017 in Riverton (U.S. Department of Energy, 2019). In addition, the relative moments and reactivity indices of these evaporitic constituents were close to that of uranium, and sulfate during both floodings and with chloride during Flood-1 (Table S4). These results further indicated uranium-rich sulfate evaporite dissolution as the predominant contaminant release from the vadose zone during both floodings, with chloride evaporites contributing primarily during Flood-1.

While both chloride- and sulfate-rich evaporite salts are soluble upon contact with water, chloride salts dissolve faster than sulfate salts during the re-solution stage (Drever, 1982). In contrast, chloride salts precipitate slower than sulfate salts during the dry stage (Armellini et al., 1994). Thus, it is possible that the chloride evaporite salts that were present in the vadose zone prior to our flooding experiments, dissolved away faster than sulfate evaporites during Flood-1. There was a one-year interval between the two flooding experiments which might not be enough for chloride evaporite salts to fully precipitate in the vadose zone before Flood-2. Consequently, less chloride release was observed during Flood-2.

### 3.4. Impact of added alkalinity

Since the primary contaminant at our study site is uranium (Dam et al., 2015), alkalinity was added during Flood-2 to determine whether this addition could remediate the contaminated site by accelerating uranium flushing from the vadose zone. Moreover, the accumulated secondary uranium mass that persists in the vadose zone, mostly in association with evaporites, can maintain a dissolved contaminant plume for numerous millennia at uranium-contaminated sites. This persistence occurs even after approximately 99% of the primary uranium mass has been removed from the surface (Kent et al., 2024), as observed at the Riverton site (Dam et al., 2015). In addition, the groundwater downgradient of the Riverton site remains contaminated despite large flooding and recharge events in 2010, 2016, and 2017 (U.S. Department of Energy, 2019). This observation further supports the persistence of uranium-associated evaporites in the vadose zone and the continuous contamination of groundwater from the vadose zone. Thus, during Flood-2, an additional 1553 mg/L $NaHCO_3$ was mixed with the flood water for remediation purpose (Table 1). The added alkalinity was 1.8 times higher than that of pre-flooding groundwater which was 550 mg/L as $CaCO_3$ (Table S2). High bicarbonate concentration was previously found to increase uranium desorption rate due to formation of aqueous U-$CO_3$ species (Alam and Cheng, 2014; Liu et al., 2017). U(VI) is far more mobile than U(IV) and the mobility of U(VI) is enhanced by the relatively high carbonate concentrations characteristic of many alkaline systems (Dong and Brooks, 2006; Qafoku and Icenhower, 2008).

During Flood-2, the mobilized uranium mass from the vadose zone was slightly higher (24%) than it was in Flood-1 (21%) (Fig. 8). The results suggested the added alkalinity might have an impact on increased uranium mobility during Flood-2. However, the pattern and concentration of alkalinity was observed to be almost identical to that of expected during the flooding event (Fig. S7) with pH in range of about 7–7.4. The results indicated that, despite the added alkalinity, the net addition of uranium to the groundwater during Flood-2 was not significantly higher, albeit solid-phase uranium concentrations before Flood-2 were unknown. Thus, the effectiveness of added alkalinity on uranium mobilization could not be determined with confidence. It is noteworthy that an excess alkalinity injection could cause more uranium retardation than desorption via uranium coprecipitation with calcite (Chen et al., 2016; Dangelmayr et al., 2023). Thus, the possibility of a certain amount of uranium retardation during Flood-2 with added alkalinity cannot be disregarded. The above results suggested that added alkalinity might not be an effective remediation technique for a uranium-contaminated site with uranium in the vadose zone.

## 4. Conclusions

This study experimentally simulated two flooding events at a field scale, to characterize contaminant mobility during natural flooding events. It was hypothesized that the contaminant mobilization from the vadose zone was due to contaminant-rich evaporite dissolution during a flooding event. The current study clearly established that the vadose zone serves as a long-term source for contaminant release during flooding events. Additionally, the study identified two primary mobilization mechanisms of contaminants from the vadose zone - (1) physical mobilization attributing to the release of contaminant-rich pore water from the vadose zone, and (2) chemical mobilization attributing to the dissolution of contaminant-rich evaporite minerals that accumulated in the vadose zone sediments. The study was inconclusive with regard to effectiveness added alkalinity as a remediation measure in a field setting, particularly for uranium, and was unable not determine whether contaminant-rich pore water originated from the unsaturated zone or the capillary fringe layer. Nonetheless, our findings have important implications for plume monitoring as they contribute to identifying secondary source locations and understanding the processes governing the release of contaminants during flooding events. Our study documented the release of contaminants from the vadose zone, with findings from our flooding experiments potentially transferable to other unconfined granular porous media. The findings from this study will better inform reactive transport models by pinpointing the primary mechanisms responsible for contaminant mobilization from the vadose zone during flooding events. This refined understanding will, in return, improve the predictive capabilities of future reactive transport models.

## Funding

The authors express their sincere gratitude for the financial support from the National Science Foundation (NSF) under award number: 2229869 and the 2022 Geological Society of America (GSA) Graduate Student Research Grant: 13597-22.

## CRediT authorship contribution statement

**Rakiba Sultana:** Writing – original draft, Investigation, Funding acquisition, Formal analysis, Conceptualization. **Raymond H. Johnson:** Writing – review & editing, Project administration, Methodology, Funding acquisition, Conceptualization. **Aaron D. Tigar:** Investigation, Data curation. **Timothy J. Wahl:** Investigation, Data curation. **Cullen E. Meurer:** Investigation. **Kendyl N. Hoss:** Investigation. **Shangping Xu:** Writing – review & editing. **Charles J. Paradis:** Writing – review & editing, Supervision, Methodology, Funding acquisition, Conceptualization.

## Declaration of competing interest

The authors declare that they have no known competing financial interests or personal relationships that could have appeared to influence the work reported in this paper.

## Data availability

Data will be made available on request.

## Acknowledgements

The authors would like to thank the U.S. Department of Energy Office of Legacy Management for their invaluable support with site access, personnel, and funding to conduct field experiments, and overall technical assistance, provided through contract #DE-LM0000421 with Navarro Research and Engineering, Inc. (through March 30, 2021) and contract #89303020DLM000001 with RSI EnTech, LLC (after April 1, 2021).

## Appendix A. Supplementary data

Supplementary data to this article can be found online at https://doi.org/10.1016/j.jconhyd.2024.104391.

## References

Aiken, M.L., Ying, S.C., 2023. Small community water systems have the highest prevalence of Mn in drinking water in California, USA. ACS EST Water 3, 2168–2178. https://doi.org/10.1021/acsestwater.3c00007.

Alam, Md.S., Cheng, T., 2014. Uranium release from sediment to groundwater: influence of water chemistry and insights into release mechanisms. J. Contam. Hydrol. 164, 72–87. https://doi.org/10.1016/j.jconhyd.2014.06.001.

Amiaz, Y., Sorek, S., Enzel, Y., Dahan, O., 2011. Solute transport in the vadose zone and groundwater during flash floods. Water Resour. Res. 47 https://doi.org/10.1029/2011WR010747, 2011WR010747.

Apaydın, A., Aktaş, S.D., 2012. Assessment of groundwater quality of the Tatlicay aquifer and relation to the adjacent evaporitic formations (Cankiri, Turkey). Environ. Monit. Assess. 184, 2337–2357. https://doi.org/10.1007/s10661-011-2121-8.

Armellini, F.J., Tester, J.W., Hong, G.T., 1994. Precipitation of sodium chloride and sodium sulfate in water from sub- to supercritical conditions: 150 to 550 °C, 100 to

300 bar. J. Supercrit. Fluids 7, 147–158. https://doi.org/10.1016/0896-8446(94)90019-1.
Barber, L.B., Paschke, S.S., Battaglin, W.A., Douville, C., Fitzgerald, K.C., Keefe, S.H., Roth, D.A., Vajda, A.M., 2017. Effects of an extreme flood on trace elements in river water—from urban stream to Major River basin. Environ. Sci. Technol. 51, 10344–10356. https://doi.org/10.1021/acs.est.7b01767.
Benito, G., Rohde, R., Seely, M., Külls, C., Dahan, O., Enzel, Y., Todd, S., Botero, B., Morin, E., Grodek, T., Roberts, C., 2010. Management of Alluvial Aquifers in two southern African ephemeral Rivers: implications for IWRM. Water Resour. Manag. 24, 641–667. https://doi.org/10.1007/s11269-009-9463-9.
Bowman, R.S., Gibbens, J.F., 1992. Difluorobenzoates as nonreactive tracers in soil and ground water. Ground Water 30, 8–14. https://doi.org/10.1111/j.1745-6584.1992.tb00805.x.
Callahan, T.J., Reimus, P.W., Bowman, R.S., Haga, M.J., 2000. Using multiple experimental methods to deter-mine fracture/matrix interactions and dispersion of non-reactive solutes in saturated volcanic tuff. WaterResour. Res. 36 (12), 3547–3558.
Carlisle, D., Merifield, P.M., Orme, A.R., Kohl, M.S., Kolker, O., Lunt, O.R., 1978. Distribution of Calcretes and Gypcretes in Southwestern United States and their Uranium Favorability, Based on a Study of Deposits in Western Australia and soUth West Africa (Namibia) (No. GJBX-29(78), 5049447). https://doi.org/10.2172/5049447.
Chen, X., Romaniello, S.J., Herrmann, A.D., Wasylenki, L.E., Anbar, A.D., 2016. Uranium isotope fractionation during coprecipitation with aragonite and calcite. Geochim. Cosmochim. Acta 188, 189–207. https://doi.org/10.1016/j.gca.2016.05.022.
Crawford, S.E., Brinkmann, M., Ouellet, J.D., Lehmkuhl, F., Reicherter, K., Schwarzbauer, J., Bellanova, P., Letmathe, P., Blank, L.M., Weber, R., Brack, W., Van Dongen, J.T., Menzel, L., Hecker, M., Schüttrumpf, H., Hollert, H., 2022. Remobilization of pollutants during extreme flood events poses severe risks to human and environmental health. J. Hazard. Mater. 421, 126691 https://doi.org/10.1016/j.jhazmat.2021.126691.
Dahan, Ofer, Dahan, O., Shani, Yuval, Shani, Y., Enzel, Yehouda, Enzel, Y., Yechieli, Yoseph, Yechieli, Y., Yakirevich, A., Yakirevich, A., 2007. Direct measurements of floodwater infiltration into shallow alluvial aquifers. J. Hydrol. 344, 157–170. https://doi.org/10.1016/j.jhydrol.2007.06.033.
Dahan, O., Tatarsky, B., Enzel, Y., Kulls, C., Seely, M., Benito, G., 2008. Dynamics of flood water infiltration and ground water recharge in Hyperarid Desert. Groundwater 46, 450–461. https://doi.org/10.1111/j.1745-6584.2007.00414.x.
Dahan, O., Talby, R., Yechieli, Y., Adar, E., Lazarovitch, N., Enzel, Y., 2009. In situ monitoring of water percolation and solute transport using a vadose zone monitoring system. Vadose Zone J. 8, 916–925. https://doi.org/10.2136/vzj2008.0134.
Dam, W.L., Campbell, S., Johnson, R.H., Looney, B.B., Denham, M.E., Eddy-Dilek, C.A., Babits, S.J., 2015. Refining the site conceptual model at a former uranium mill site in Riverton, Wyoming, USA. Environ. Earth Sci. 74, 7255–7265. https://doi.org/10.1007/s12665-015-4706-y.
Dangelmayr, M., Meurer, C., Tigar, A., Johnson, R.H., Paradis, C., 2023. Desorption and co-dissolution of uranium-bearing solids during alkalinity-enhanced Flushing of contaminated sediments. Groundwater Monitor. Rem. gwmr.12573 https://doi.org/10.1111/gwmr.12573.
Dong, W., Brooks, S.C., 2006. Determination of the Formation Constants of Ternary Complexes of Uranyl and Carbonate with Alkaline Earth Metals ($Mg^{2+}$, $Ca^{2+}$, $Sr^{2+}$, and $Ba^{2+}$) Using Anion Exchange Method. Environ. Sci. Technol. 40, 4689–4695. https://doi.org/10.1021/es0606327.
Drever, J.I., 1982. The Geochemistry of Natural Waters. Prentice-Hall, Englewood Cliffs, N.J.
Drinking Water Regulations and Contaminants, 2024. EPA.gov. Last modified on February 14. https://www.epa.gov/sdwa/drinking-water-regulations-and-contaminants.
Du Laing, G., Vanthuyne, D.R.J., Vandecasteele, B., Tack, F.M.G., Verloo, M.G., 2007. Influence of hydrological regime on pore water metal concentrations in a contaminated sediment-derived soil. Environ. Pollut. 147, 615–625. https://doi.org/10.1016/j.envpol.2006.10.004.
Dwivedi, D., Steefel, C.I., Arora, B., Banfield, J., Bargar, J., Boyanov, M.I., Brooks, S.C., Chen, X., Hubbard, S.S., Kaplan, D., Kemner, K.M., Nico, P.S., O'Loughlin, E.J., Pierce, E.M., Painter, S.L., Scheibe, T.D., Wainwright, H.M., Williams, K.H., Zavarin, M., 2022. From legacy contamination to watershed systems science: a review of scientific insights and technologies developed through DOE-supported research in water and energy security. Environ. Res. Lett. 17, 043004 https://doi.org/10.1088/1748-9326/ac59a9.
Freeze, R.A., Cherry, J.A., 1979. Physical properties and principles. In: Groundwater. Prentice-Hall, Englewood Cliffs, N.J, pp. 38–40.
Frohne, T., Rinklebe, J., Diaz-Bone, R.A., Du Laing, G., 2011. Controlled variation of redox conditions in a floodplain soil: impact on metal mobilization and biomethylation of arsenic and antimony. Geoderma 160, 414–424. https://doi.org/10.1016/j.geoderma.2010.10.012.
Gregory, R.W., 2019. Uranium Geology and Resources of the Gas Hills District, Wind River Basin. In: Central Wyoming: Wyoming State Geological Survey Public Information Circular, vol. 47, p. 31.
Gross, A., Besov, A., Diaz Reck, D., Sorek, S., Ben-Dor, G., Britan, A., Palchikov, E., 2003. Application of waves for remediation of contaminated aquifers. Environ. Sci. Technol. 37, 4481–4486. https://doi.org/10.1021/es026297d.
Hooda, P.S. (Ed.), 2010. Trace Elements in Soils, 1st ed. Wiley. https://doi.org/10.1002/9781444319477.
Izquierdo, M., Tye, A.M., Chenery, S.R., 2017. Using isotope dilution assays to understand speciation changes in cd, Zn, Pb and Fe in a soil model system under simulated flooding conditions. Geoderma 295, 41–52. https://doi.org/10.1016/j.geoderma.2017.02.006.
Johnson, R.H., Dam, W.L., Campbell, S., Noël, V., Bone, S.E., Bargar, J.R., Dayvault, J., 2016. Persistent secondary contaminant sources at a former uranium mill site, Riverton, Wyoming, USA. In: Proceedings IMWA 2016. Presented at the Mining Meets Water – Conflicts and Solutions, Freiberg/Germany, pp. 398–404.
Keefer, W.R., 1970. Structural Geology of the Wind River Basin, Wyoming (No. 495- D). Prepared in Cooperation with The Geological SURVEY of Wyoming and the Department of Geology of the University of Wyoming as Part of a Program of the Department of the Interior for development of the Missouri River basin.
Kent, R.D., Johnson, R.H., Laase, A.D., Nyman, J.L., 2024. Modeling evaluation of the impact of residual source material on remedial time frame at a former uranium mill site. J. Contam. Hydrol. 261, 104298 https://doi.org/10.1016/j.jconhyd.2024.104298.
Knowlton Jr., R.G., Peterson, D.M., Zhang, H., 1997. Analysis of Natural Attenuation as the Preferred Ground Water Alternative at the DOE UMTRA Site near Riverton. Sandia National Laboratories, WY.
Langmuir, D., 1977. Uranium Solution-Mineral Equilibria at Low Temperatures with Applications to Sedimentary Ore Deposits (No. GJO-1659-3, GJBX-54(78), 6774931). https://doi.org/10.2172/6774931.
Liu, B., Peng, T., Sun, H., Yue, H., 2017. Release behavior of uranium in uranium mill tailings under environmental conditions. J. Environ. Radioact. 171, 160–168. https://doi.org/10.1016/j.jenvrad.2017.02.016.
Looney, B.B., Denham, M.E., Eddy-Dilek, C.A., 2014. Independent Technical Evaluation and Recommendations for Contaminated Groundwater at the Department of Energy Office of Legacy Management Riverton Processing Site (No. SRNL-STI–2014-00163, 1130785). https://doi.org/10.2172/1130785.
Mackay, D.M., Einarson, M.D., Kaiser, P.M., Nozawa-Inoue, M., Goyal, S., Chakraborty, I., Rasa, E., Scow, K.M., 2012. Mass discharge in a tracer plume: evaluation of the Theissen polygon method. Groundwater 50, 895–907. https://doi.org/10.1111/j.1745-6584.2012.00912.x.
Management, D.L., 2016. Uranium-bearing Evaporite mineralization influencing plume persistence. In: Literature Review and DOE-LM Site Surveys. LMS/S13437; ESL-RPT-2015-05.
Miao, Z., Brusseau, M.L., Carroll, K.C., Carreón-Diazconti, C., Johnson, B., 2012. Sulfate reduction in groundwater: characterization and applications for remediation. Environ. Geochem. Health 34, 539–550. https://doi.org/10.1007/s10653-011-9423-1.
Narasimhan, T.N., White, A.F., Tokunaga, T., 1986. Groundwater contamination from an inactive uranium mill tailings pile: 2. Application of a dynamic mixing model. Water Resour. Res. 22, 1820–1834. https://doi.org/10.1029/WR022i013p01820.
National Primary Drinking Water Regulations, 2024. EPA.gov. Last Modified on January 2 epa.gov/ground-water-and-drinking-water/national-primary-drinking-water-regulations.
Nativ, R., Adar, E., Dahan, O., Geyh, M., 1995. Water recharge and solute transport through the vadose zone of fractured chalk under desert conditions. Water Resour. Res. 31, 253–261. https://doi.org/10.1029/94WR02536.
Paradis, C., Sultana, R., 2024. Tracer-based separation of advection and dispersion from breakthrough curves. Geosci. Facult. Articl. 28.
Paradis, C.J., Dixon, E.R., Lui, L.M., Arkin, A.P., Parker, J.C., Istok, J.D., Perfect, E., McKay, L.D., Hazen, T.C., 2019. Improved method for estimating reaction rates during push-pull tests. Groundwater 57, 292–302. https://doi.org/10.1111/gwat.12770.
Paradis, C.J., Johnson, R.H., Tigar, A.D., Sauer, K.B., Marina, O.C., Reimus, P.W., 2020. Field experiments of surface water to groundwater recharge to characterize the mobility of uranium and vanadium at a former mill tailing site. J. Contam. Hydrol. 229, 103581 https://doi.org/10.1016/j.jconhyd.2019.103581.
Paradis, C.J., Hoss, K.N., Meurer, C.E., Hatami, J.L., Dangelmayr, M.A., Tigar, A.D., Johnson, R.H., 2022a. Elucidating mobilization mechanisms of uranium during recharge of river water to contaminated groundwater. J. Contam. Hydrol. 251, 104076 https://doi.org/10.1016/j.jconhyd.2022.104076.
Paradis, C., Van Ee, N., Hoss, K., Meurer, C., Tigar, A., Reimus, P., Johnson, R., 2022b. Single-well injection-drift test to estimate groundwater velocity. Groundwater 60, 565–570. https://doi.org/10.1111/gwat.13184.
Ponting, J., Kelly, T.J., Verhoef, A., Watts, M.J., Sizmur, T., 2021. The impact of increased flooding occurrence on the mobility of potentially toxic elements in floodplain soil – a review. Sci. Total Environ. 754, 142040 https://doi.org/10.1016/j.scitotenv.2020.142040.
Qafoku, N.P., Icenhower, J.P., 2008. Interactions of aqueous U(VI) with soil minerals in slightly alkaline natural systems. Rev. Environ. Sci. Biotechnol. 7, 355–380. https://doi.org/10.1007/s11157-008-9137-8.
Ricker, J.A., 2008. A practical method to evaluate ground water contaminant plume stability. Ground Water Monit. Remidiat. 28, 85–94. https://doi.org/10.1111/j.1745-6592.2008.00215.x.
Simpson, S.C., Meixner, T., Hogan, J.F., 2013. The role of flood size and duration on streamflow and riparian groundwater composition in a semi-arid basin. J. Hydrol. 488, 126–135. https://doi.org/10.1016/j.jhydrol.2013.02.049.
Singh, G., Şengör, S.S., Bhalla, A., Kumar, S., De, J., Stewart, B., Spycher, N., Ginn, T.M., Peyton, B.M., Sani, R.K., 2014. Reoxidation of biogenic reduced uranium: a challenge toward bioremediation. Crit. Rev. Environ. Sci. Technol. 44, 391–415. https://doi.org/10.1080/10643389.2012.728522.
Sorek, S., 1996. A model for solute transport following an abrupt pressure impact in saturated porous media. Transp. Porous Media 22, 271–285. https://doi.org/10.1007/BF00161627.

Sorek, S., Bear, J., 1990. Evolution of governing mass and momentum balances following an abrupt pressure impact in a porous medium. Transp. Porous Media 5, 169–185. https://doi.org/10.1007/BF00144602.

Truex, M.J., Oostrom, M., Brusseau, M.L., 2009. Estimating persistent mass flux of volatile contaminants from the vadose zone to ground water. Groundwater Monitor. Rem. 29, 63–72. https://doi.org/10.1111/j.1745-6592.2009.01236.x.

U.S. Department of Energy, 1998. Final Site Observational Work Plan for the UMTRA Project Site at Riverton, Wyoming, Report No. U0013801.

U.S. Department of Energy, 2016. 2015 Advanced Site Investigation and Monitoring Report Riverton, Wyoming, Processing Site September 2016 (No. S–14148, 1351628). https://doi.org/10.2172/1351628.

U.S. Department of Energy, 2019. Three Years of Multilevel Monitoring Data at the Riverton, Wyoming, Processing Site That Show Contaminant Increases After River Flooding Events and a Large Recharge Event (No. LMS/RVT/S26137). Office of Legacy Management.

U.S. Department of Energy, 2023. Applied Studies and Technology Persistent Secondary Contaminant Sources Data Release from Field Tracer Testing Studies at the Riverton, Wyoming, Processing Site (No. LMS/ESL/43015), AS&T- Persistent Secondary Contaminant Sources Data Release, Field Tracer Testing Studies at Riverton Site.

U.S. Department of Energy, L.M, 2014. Evaluation of Mineral Deposits along the Little Wind River. Riverton, Wyoming, Processing Site.

Warrick, A.W., Biggar, J.W., Nielsen, D.R., 1971. Simultaneous solute and water transfer for an unsaturated soil. Water Resour. Res. 7, 1216–1225. https://doi.org/10.1029/WR007i005p01216.

Weber, F.-A., Voegelin, A., Kretzschmar, R., 2009. Multi-metal contaminant dynamics in temporarily flooded soil under sulfate limitation. Geochim. Cosmochim. Acta 73, 5513–5527. https://doi.org/10.1016/j.gca.2009.06.011.

White, A.F., Delany, J.M., Narasimhan, T.N., Smith, A., 1984. Groundwater contamination from an inactive uranium mill tailings pile: 1. Application of a chemical mixing model. Water Resour. Res. 20, 1743–1752. https://doi.org/10.1029/WR020i011p01743.

Yabusaki, S.B., Wilkins, M.J., Fang, Y., Williams, K.H., Arora, B., Bargar, J., Beller, H.R., Bouskill, N.J., Brodie, E.L., Christensen, J.N., Conrad, M.E., Danczak, R.E., King, E., Soltanian, M.R., Spycher, N.F., Steefel, C.I., Tokunaga, T.K., Versteeg, R., Waichler, S.R., Wainwright, H.M., 2017. Water table dynamics and biogeochemical cycling in a shallow, variably-saturated floodplain. Environ. Sci. Technol. 51, 3307–3317. https://doi.org/10.1021/acs.est.6b04873.

Yang, F., Yue, S., Wu, X., Zhang, C., Li, D., Zhu, R., 2023. Effects of flood inundation on biogeochemical processes in groundwater during riverbank filtration. J. Hydrol. 617, 129101 https://doi.org/10.1016/j.jhydrol.2023.129101.